A novel collaborative multiscale weighting factor-adaptive Kalman filtering method for the time-varying whole-life-cycle state of charge estimation of lithium-ion batteries.

WANG, S., FAN, Y., YU, C., JIN, S., TAKYI-ANINAKWA, P., FERNANDEZ, C. and STROE, D.-I.

2022

A novel collaborative multiscale weighting factor-adaptive Kalman filtering method for the time-varying whole-life-cycle state of charge estimation of lithium-ion batteries

Shunli Wang[1], Yongcun Fan[1], Chunmei Yu[1], Siyu Jin[2], Paul Takyi-Aninakwa[1], Carlos Fernandez[3], Daniel-Ioan Stroe[2]

[1]School of Information Engineering & Robot Technology used for Special Environment Key Laboratory of Sichuan Province, Southwest University of Science and Technology, Mianyang, 621010, China. [2]Department of Energy Technology, Aalborg University, Pontoppidanstraede, 111 9220 Aalborg East, Denmark. [3]School of Pharmacy and Life Sciences, Robert Gordon University, Aberdeen AB10-7GJ, UK.

Abstract: Accurate state of charge (SOC) estimation is essential for the whole-life-cycle safety guarantee and protection of lithium-ion batteries, which is quite difficult to realize. In this study, a novel weighting factor-adaptive Kalman filtering (WF-AKF) method is proposed for the accurate estimation of SOC with a collaborative model for parameter identification. An improved bipartite electrical equivalent circuit (BEEC) model is constructed to describe the dynamic characteristics combined with the mathematical correction of the time-varying factors. The model parameters are identified online, corresponding to various SOC levels and temperature conditions. Considering the internal resistances, ambient temperature, and complex current rate variations, an adaptive multi-time scale iterative calculation model is constructed and combined with the real-time estimation and correction strategies. The maximum closed-circuit voltage (CCV) traction error is 0.36% and 0.24% for the main pulse-current charging and discharging processes, respectively. The proposed WF-AKF algorithm stabilizes the large initial SOC estimation error by tracking the actual value with a maximum error of 0.46% under the complex working condition. The SOC estimation is accurate and robust to the time-varying characteristics and working conditions even when the initial error is large, providing a safety protection theory for lithium-ion batteries.

Keywords: lithium-ion battery; whole-life-cycle; state of charge estimation; collaborative bipartite electrical equivalent circuit model; time-varying characteristics; weighting factor-adaptive Kalman filter

Corresponding authors: Shunli Wang, wangshunli@swust.edu.cn.

Highlights

- A novel weighting factor-adaptive Kalman filtering (WF-AKF) method is proposed for the whole-life-cycle state of charge (SOC) estimation of lithium-ion batteries.
- The improved collaborative bipartite electrical equivalent circuit (BEEC) model is constructed by considering the time-varying factors.
- An adaptive multi-time scale model is built with real-time estimation and correction strategies.
- Multiple influencing factors are taken into consideration, including internal parameters, ambient temperature, and current rate variation.
- The proposed WF-AKF algorithm stabilizes the large initial SOC estimation error by tracking the actual value with a maximum error of 0.46% under time-varying ambient temperatures, current rates, and complex working condition.

1. Introduction

Lithium-ion batteries are effective solutions to the wide temperature range energy storage and consumption problems due to their high energy density, long lifespan, and large output power advantages. The battery system has wide application potential that can effectively promote the economy and social security [1]. There is a critical need to realize a reliable battery energy supply and instantaneous power output. The state of charge (SOC) condition influences the battery life cycle and service capabilities, which has become a hot issue [2]. As wide temperature range reliability research is still in its infant stage, the theory and available technologies cannot meet the social development requirements. So, the accuracy of the SOC estimation becomes a bottleneck that restricts economic progress.

As a complex electrochemical system, an accurate battery equivalent circuit model is quite difficult to establish. Therefore, effective approaches are proposed to solve these challenges, and experimental methodologies are discussed for subsequent chemical and physical characteristics, electrochemical dynamics, thermodynamic analysis, accuracy, and validity [3]. The development of technology faces setbacks due to severe challenges and a wide outstanding technological level gap that needs improvement to ensure high sustainability [4]. An electrical equivalent circuit model (ECM) is necessary to obtain the battery characteristics. The mathematical expression is a prerequisite for reliable SOC estimation, which is conducted for accurate SOC estimation with the state-space equation of the ECM model [5]. As for the asymptotic reduction and homogenization, a thermo-electrochemical model is constructed [6]. By building a physics-based model, the SOC estimation is realized by considering the battery aging characteristics [7]. Continuous modeling is conducted for cyclic aging [8]. Adaptive fusion estimation algorithms are proposed by considering the wide operating temperature range and degradation [9]. Dynamic ECMs and the differential Kalman filter are investigated under time-varying conditions [10]. A time-domain ECM is conducted using low-frequency electrochemical impedance spectroscopy [11]. An investigation of capacity fading model is conducted when the battery is cycled at different SOC levels [12]. Consequently, the enhanced ECM is used for the charging redistribution and temperature variation, in which the parameter identification is investigated by considering the electrochemical characteristics.

The battery's behavior is expressed with mathematical expressions using circuit elements, including voltage, current, resistances, capacitances, and inductances [13]. The electrical ECM is also combined with the simplified electrochemical model by introducing a concentrated structure to realize the state-space equation [14]. This modeling type includes electronic components and circuits so that the system-level design and physical modeling parameters are intuitive, according to which an improved cuckoo search particle filter is used for the SOC estimation [15]. The co-estimation of SOC and state of temperature (SOT) is realized with a hybrid thermal

electrochemical neural network model [16]. Based on the modeling characteristic analysis, an ECM is constructed, and the thermal behavior is described by a state-space equation.

The model parameter identification is conducted to explore the global optimization strategies. Model-based state estimation is conducted, and the corresponding parameters are identified by conducting hybrid pulse- power characterization (HPPC) tests [17]. The parameter identification problem is overcome with an electrochemical model by constructing adaptive observers [18]. Afterward, the demonstration is applied to the battery cells, including the SOC estimation conducted by the extended Kalman filter [19]. The SOC estimation is also conducted by building an intelligent adaptive extended Kalman filter with an improved noise estimator [20]. The global optimization methods are analyzed comparatively for model parameter identification [21]. The parameter sensitivity is evaluated, and the coupling model is built for the cyclic SOC estimation to obtain the degradation status [22]. Based on the relationship between the current rate and terminal voltage, improved resistor-capacitor circuits are used to express the internal characteristics with the voltage hysteresis.

After the model is built, it is necessary to conduct parameter identification for the model. Real-time entropy estimation based on a Kalman filter is conducted when it is combined with a nonlinear observer [23]. A novel identification method is proposed based on second-order resistor-capacitor ECM parameters to describe the battery's transient characteristics [24]. The discharge mode identification is conducted for the online SOC estimation of series-connected battery packs [25]. The OCV estimation algorithm is used for parameter identification [26]. The online capacity estimation is conducted using a deep long short-term memory network [27]. Adaptive model parameter identification for lithium-ion batteries is based on an improved coupling hybrid adaptive particle swarm optimization and the simulated annealing method [28]. The parameter changing factors are extracted and introduced into the iterative calculation process, and the distribution is simulated from important micro-physical quantities obtained with high fidelity.

Precise modeling is essential to describe the relationship between various state parameters, according to which the working condition's influence is considered for both the temperature and aging degree. The dynamic partial equations are used to describe the mechanism of the internal reaction of lithium-ion batteries [29]. The mechanism analyzes the lithium-ion concentration and potential distribution, which is then utilized to calculate the real-time internal reaction rate [30]. The electrochemical reaction is simulated accurately with a complex structure, as too many parameters should be identified using the results of experimental tests [31]. Simplified electrochemical models are used in real-time applications so that the internal mechanisms are described by electrochemical reactions by constructing the empirical equations [32]. Voltage and current are used to describe the battery's characteristics and mathematical notations. The computational complexity is reduced accordingly, so that the accuracy is improved by the simplification method.

The parameter identification accuracy is directly affected by the application efficiency under complex and variable temperature conditions. The influence of the ambient temperature and aging characteristics are introduced into the modeling processes [33]. As the offline parameter identification cannot reflect the full life battery information accurately, the online parameter identification is realized to improve the estimation accuracy by considering the wide temperature range influence [34]. The ECM is combined with the external measurable parameters under complex working scenarios, and the cell-to-cell consistency difference is suppressed by the noise interference [35]. The charge-discharge efficiency varies with temperature and current rate variation. As the available capacity is reduced when the temperature is low, the estimated value is revised constantly by considering the influence of aging and self-discharge factors [36]. Under the wide-temperature range influence, there is noise in the measured value of external electrical parameters, so the feature information extraction is difficult, including mathematical modeling and state estimation [37]. Collaborative SOC attenuation and wide temperature range state estimation become the keys to achieving reliable application, improving energy utilization efficiency, service life

extension, and safety insurance [38]. The neural network is also used to describe the non-linear characteristics of lithium-ion batteries suitable for state estimation [39]. A large number of training samples are required to correct the training data difference and accuracy affecting functions [40]. The large computation requires a powerful processing chip, so the energy management is focused on the various random collection models.

Model parameters are identified to solve the influencing factor correction problem, according to which the estimation accuracy is improved by the modified unscented Kalman filter (UKF) for the adaptive modeling of multiple current rate conditions. The model capacity degradation is conducted, and the block diffusion modeling is conducted under dynamic working conditions [41]. The pruned convolutional neural network approach is proposed by the capacity estimation that is assisted with transfer learning [42]. The optimized state estimation is supposed to realize the automotive tests by the adaptive management of the battery safety protection [43]. The high-speed temperature sensor is also introduced to monitor the working state of batteries with low supply sensitivity, which benefits the present application and non-functional requirements [44]. Markov-based state estimation is conducted to characterize the charging process, and modular-fault tolerant processing is investigated for the mathematical state-space equation [45]. Various operating strategies are analyzed for the battery's redox performance with structural optimization.

The SOC estimation accuracy should be improved due to its influence on the battery management systems. An enhanced multi-state estimation hierarchy is constructed for advanced battery management systems [46]. The deep convolutional neural networks are constructed and combined with ensemble learning and transfer learning [47]. A hybrid statistical data-driven method is proposed for the online joint state estimation [48]. An adaptive square root- extended Kalman filter is constructed for SOC estimation in complex conditions [49]. An improved cubature Kalman filter is constructed, and combined with a long short-term memory model for the packing SOC estimation [50]. As an essential parameter, effective identification is conducted to improve the whole-life-cycle

battery performance and support the energy supply optimization by utilizing noise measurement and multilayer invariant localization.

The angular velocity is performed through sliding-window nonlinear optimization using a semi-tightly coupled integration scheme with seamless navigation. Through sliding-window nonlinear optimization, the angular velocity is performed, and the optimization is realized using a semi-tightly coupled integration scheme with seamless navigation. An efficient nonlinear cubature Kalman filter (CKF) is conducted for visual-inertial iodometry, and a state observer is built by complex sensor fusion [51]. Accurate classification of time-series data is realized by the extended application of fault diagnosis, in which the interconnected state observer is constructed by electrochemical modeling [52]. The internal ohmic resistance calculation is combined with the state of health degree, establishing a multi-index estimation system for the regressive battery state estimation. The differential evolution models are conducted, and the fractional-order incremental analysis is performed [53]. The state estimation availability is highly dynamic due to time-varying factors, including energy variation, life decay, and charge-discharge current rate variation.

The state observation shows unique advantages in non-Gaussian models that have strong modeling capabilities for the nonlinear characteristics of time-varying battery parameters. A performance evaluation is carried out where the ratio of measured and rated capacity is calculated when the battery is fully charged [38]. The reliability of the power supply capability is set as a manifestation, and a series of micro-short circuit diagnoses are conducted with a mean-difference model [54]. Significant results are achieved for the model-based SOC estimation with the whole-life-cycle fading trajectory estimation that can meet the urgent requirements effectively for the reliable battery system application [55]. The maximum available capacity is combined with the least-squares algorithm based on dual capacity estimation [56]. The high-fidelity capacity degradation model is constructed to reflect battery internal activity, which is combined with chemical kinetics to identify model parameters, making the

model adaptive to the battery aging process.

Under complex working condition, the capacity decay effect mechanism is investigated to optimize the power resource scheduling by considering the research dynamics and urgent practical application requirements. Subsequently, a novel weighting factor-adaptive Kalman filtering (WF-AKF) method is proposed for the whole-life-cycle SOC estimation of lithium-ion battery packs. Through real-time experimental data acquisition in the fractional calculus, an improved bipartite electrical equivalent circuit (BEEC) model is established, providing a spatial equation suitable for state estimation. The WF-AKF-based collaborative estimation is conducted for both the SOC and model parameters with the equivalent circuit modeling process, providing scientific evidence for the reliable lithium-ion battery application.

2. Mathematical analysis

The working environment and aging characteristics are considered under wide temperature range conditions, according to which the collaborative SOC estimation is realized with the model parameter identification. An iterative calculation model is established for the full-life-cycle battery state estimation with an adaptive correction capability under wide temperature range conditions. The energy supply efficiency is improved effectively by promoting the adaptive model parameter estimation, which is used to describe the cell-to-cell difference. Collaborative estimation and correction are investigated to obtain mathematical methods for the dynamic battery characteristic description, which is carried out by ECM and state estimation with performance evaluation.

2.1. Discrete digital aging characteristic modeling

Under a dynamic working condition, the instantaneous power supply capacity and duration have time-varying characteristics, so the BEEC model is established. A collaborative SOC estimation scheme is designed to realize

effective residual power monitoring and optimization. After analyzing the discrete digital sampling error, the noise influence of the external measurable parameters is considered in the modeling process, and the key time-varying factors are identified. Then, the battery performance evaluation is conducted, and a full life-feature model is established accordingly. The state-space equations are obtained with the output parameters under different working conditions. The changing characteristics are expressed in terms of temperature and internal ohmic resistance variations. A whole-life-cycle ECM is constructed for the experimental verification of the voltage characteristics, according to which the output voltage variation is discussed effectively. Based on this model, the composite model is constructed, and a structured circuit optimization strategy is realized through component distribution adjustment. Then, a mathematical expression is obtained by considering both equivalent circuit modeling complexities and accuracy.

The proposed ECM uses an ideal voltage source U_{oc} to characterize the open-circuit voltage (OCV). An accurate mathematical description of the self-discharge effect is realized by adding a parallel resistor R_s across the U_{oc}, thereby reducing the error effect influenced by the self-discharge phenomenon. A first-order resistor-capacitor circuit is used to describe the polarization effects and improve the battery state characterization accuracy. Considering the difference between internal-connected battery cells in the equivalent circuit modeling process, the state of balance (SOB) effect on the output voltage $U_L(L)$ is characterized by the reverse series-connected time-varying voltage source U. Then, the time-varying resistor R is used to describe the resistance variation with the internal ohmic resistance R_0. An effective model is constructed with the state-space equation by considering the influence of these factors comprehensively. The proposed BEEC model is constructed, as shown in Figure 1.

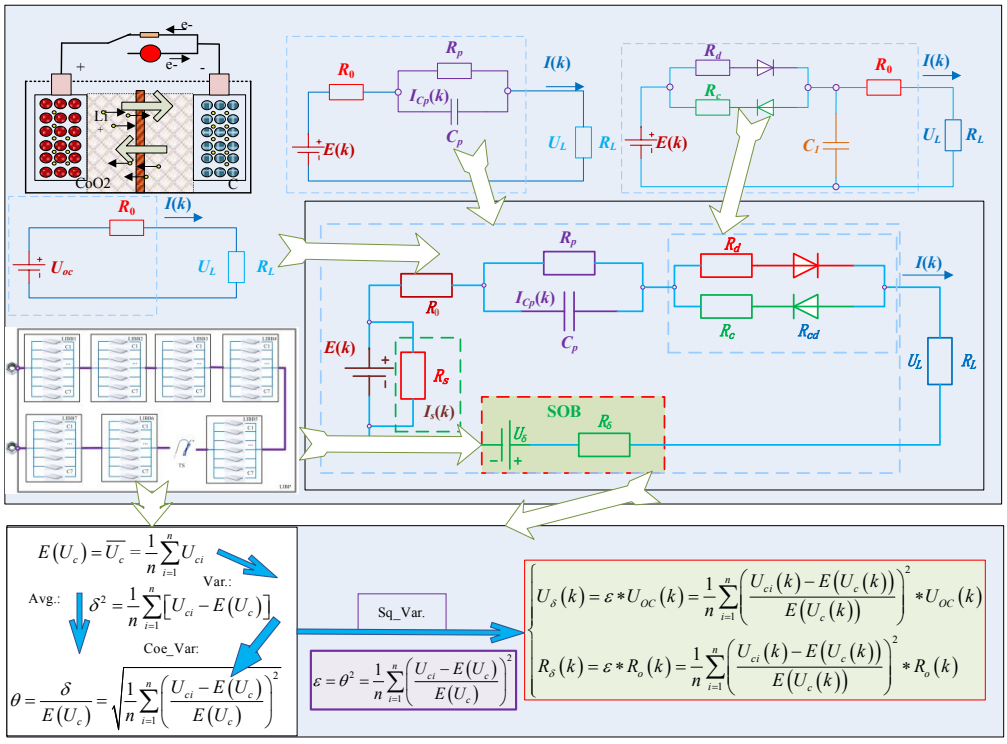

Figure 1. Schematic diagram of the BEEC model and SOB evaluation

In Figure 1, the model parameters are described as follows: R_p and C_p are used to form a first-order resistor-capacitor network to simulate the dynamic polarization characteristics. U and R are used to characterize the SOB effect and describe the internally cascaded cell-to-cell differences in the battery pack. The mathematical description of the dynamic characteristics is realized by improving the ECMs based on the exploration of the improved modeling methods with error suppression. The whole iterative calculation process includes estimation and correction. The self-discharge current is $I_s(L)$, and the mathematical expression is obtained using R_s to record the self-discharge resistance. Considering the effect of R_s, the data processing is conducted for the discrete-time calculation, so the state equation is discretized accordingly, as shown in Equation (1).

$$\begin{cases} S(k) = S(0) - \int_0^k \frac{\eta_I \eta_T I(\tau)}{Q_n} d\tau - \int_0^k \frac{I_s(\tau)}{Q_n} d\tau = S(0) - \int_0^k \frac{\eta_I \eta_T I(\tau)}{Q_n} d\tau - \int_0^k \frac{E(\tau)}{R_s Q_n} d\tau \\ S(k|k-1) = S(k-1) - \frac{\eta_I \eta_T I(k) T_s}{Q_n} - K_s * T_s \end{cases} \tag{1}$$

In Equation (1), $S(k)$ is the SOC value at the time point k; $S(0)$ is the initial SOC value; η_I is the

Coulombic efficiency for the current I; η_T is the Coulombic efficiency for the temperature T; $I(\tau)$ is the current for the time point τ; Q_n is the rated capacity of the battery; $I_s(\tau)$ is the self-discharge current; $E(\tau)$ is the electrodynamic potential difference; R_s is the internal self-discharge resistance; $S(k|k-1)$ is the estimated SOC value at the time point k from time point $k-1$; k is current discrete-time point; $S(k-1)$ is the SOC value at the time point $k-1$; $I(k)$ is output current; T_s is the discrete-time sampling period. The self-discharge influencing change is described by the parameter K_s for the measurement period. The state-space equation for the BEEC model is shown in Equation (2).

$$(R_0 + R_\delta)I(k) + U_p + I(k)R_{cd} = E(k) - U_\delta(k) - U_L(k) \tag{2}$$

In Equation (2), R_0 is the internal ohmic resistance; R_δ is the state of balance resistance; $I(k)$ is the total current; U_p is the polarization voltage of the circuit; R_{cd} is the charge-discharge difference resistance; $U_\delta(k)$ is the state of balance voltage; $U_L(k)$ is the CCV at the time point k. $E(k)$ is the electrodynamic potential difference that has a functional relationship to the battery state variation. Its mathematical relationship is described as $E(k) = f[S(k)]$ by taking $S(k)$ as the SOC value at the time point k. During the discharging process, the value of $R_{cd}(k)$ is set to be $R_{cd}(k) = R_d$ and set to be $R_{cd}(k) = R_c$ when charging. For the parameter identification, the iterative calculation of the polarization voltage U_p is obtained at the same time point as the parallel resistor-capacitor circuit. Also, it is obtained by the input-output circuit specifications, as shown in Equation (3).

$$\begin{cases} U_L(k) = E(k) - U_\delta(k) - (R_0 + R_\delta)I(k) - U_p - I(k)R_{cd} \\ U_p(k) = I(k)R_p\left(1 - e^{\frac{-T_s}{R_pC_p}}\right) \end{cases} \tag{3}$$

In Equation (3), $U_L(k)$ is the CCV at the time point k; $E(k)$ is the electrodynamic potential difference; $U_\delta(k)$ is the state of balance voltage; R_0 is the internal ohmic resistance; R_δ is the state of balance resistance; $I(k)$ is the total current; U_p is the polarization voltage; R_{cd} is the charge-discharge difference resistance;

R_p is the polarization resistance; C_p is the polarization capacitance; T_s is the discrete-time sampling period. The identified parameters are combined with the CCV variation, which is used to obtain the observation output. K_s is change amount of each measurement period considering the self-discharge influence. Also, the observation equation is obtained by substituting the calculation of $U_p(k)$into $U_L(k)$, as shown in Equation (4).

$$U_L(k) = E(k) - U_\delta(k) - (R_0 + R_\delta)I(k) - I(k)R_p\left(1 - e^{\frac{-T_s}{R_pC_p}}\right) - I(k)R_{cd} \quad (4)$$

In Equation (4), $U_L(k)$ is the CCV; $E(k)$ is the electrodynamic potential difference; $U_\delta(k)$ is the state of balance voltage; R_0 is the internal ohmic resistance; R_δ is the state of balance resistance; $I(k)$ is the total current; R_p is the polarization resistance; C_p is the polarization capacitance; T_s is the discrete-time sampling period; R_{cd} is the charge-discharge difference resistance. The composite pulse-power test is performed to obtain the model parameters corresponding to different SOC levels when the battery is working at an ambient temperature of 25 °C. The battery is discharged for 10 s for the HPPC test. Then, it is shelved for 40 s without any electrical load. Then, it is charged to full capacity for 10 s, during which the current rate is set at 1 C for the pulse charge-discharge process. The discharge process is investigated for the current SOC value, which decreases by 0.10 sequentially. After each test, the battery is shelved to ensure thermal and electrochemical equilibrium for 40 minutes. This process is repeated at different SOC levels to obtain the response data of the voltage-current variation. The current and voltage curves in the HPPC test are obtained at 45 °C, as shown in Figure 2.

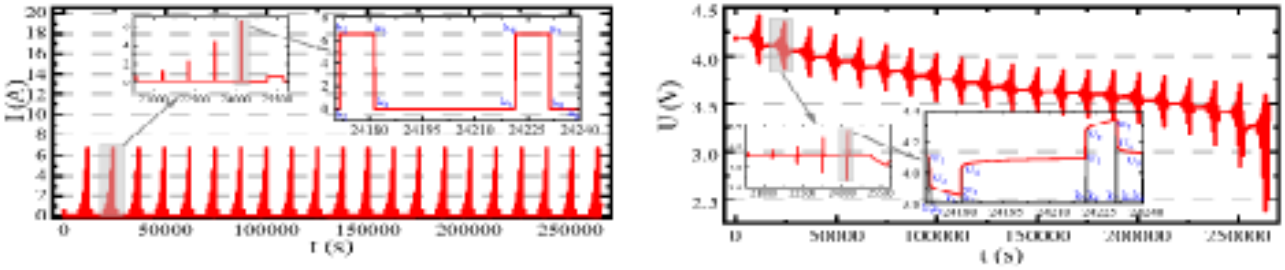

(a) Corresponding current variation (b) Corresponding voltage variation

Figure 2. Voltage-current variation under the HPPC working condition

In Figure 2., k_1 is the starting time point of the pulse charge process; k_2 is the ending and starting time point of the rapid voltage decrease and rapid voltage recovery after the pulse charge process, respectively; k_3 is the starting and ending time point of the pulse discharge process and rapid voltage recovery, respectively; k_4 is the ending and starting time point of the pulse discharge process and the slow voltage recovery, respectively; k_5 is the starting and ending time point of the pulse charge process and the slow voltage recovery, respectively; k_6 is the ending and starting time point of the pulse charge process and the rapid voltage recovery, respectively; k_7 is the starting and ending time point of the pulse discharge process and the rapid voltage recovery, respectively; k_8 is the ending and starting time point of the rapid recovery voltage after the pulse discharge process is completed; k_9 is the ending time point of the pulse discharge process and slow voltage recovery, respectively. The overall HPPC test for the varying SOC levels is expressed and the single HPPC test for SOC = 0.95 is enlarged. A detailed analysis is conducted, in which U_L increases gradually until the CCV value equals the OCV value. Corresponding battery voltage-current curves are introduced into the parameter identification process of the electrical ECM to describe the polarization effect that it related to the battery characteristics with high accuracy. By establishing a zero input-output response equation, parameter identification is realized. The pulse discharging step of 10 s in the period of k_1k_3. After that, a 40 s shelving period is conducted for k_3k_5. The segment k_5k_7 is conducted for the charging process of 10 s, and k_7k_9 is

conducted for a shelving period of 40 s.

L_1L_5 and L_5L_9 reflect the chargeand discharge characteristics, respectively, with a high symmetry effect. L_1 L_5 is demonstrated, and the analysis process for L_5L_9 is conducted similarly. (1) The L_1L_2 variation is caused by the internal ohmic resistance R_0, which is expressed at the time point when the battery is discharged. (2) U_2 U_3 is the voltage change when the polarization capacitor C_p is charged, which is a zero-input response. When circuit U_p is charged to full capacity, the voltage values at R_p and C_p are equal. (3) U_3U_4 is the voltage change when the battery is shelved. When there is no flow of current, the ohmic voltage turns to zero, and the terminal voltage rises rapidly. (4) The voltage variation in the period of U_4U_5 is due to the C_p discharging through the polarization resistor R_p, forming a zero-input response, so the voltage rises slowly. Also, the ohmic resistance R_0 is obtained by the voltage difference between U_1 and U_2, corresponding to different SOC levels. The discharging current is described by I that is obtained in the pulse charge-discharge test. The polarization resistance R_p, which is obtained by subtracting U_4 from U_5, divided by the current I, as shown in Equation (5).

$$R_0 = \frac{(U_1 - U_2)}{I}; R_p = \frac{(U_5 - U_4)}{I} \quad (5)$$

In Equation (5), R_0 is the internal ohmic resistance; R_p is the polarization resistance; U_1 is the voltage at the starting time point of discharge process; U_2 is the voltage at the ending time point of the fast discharge; I is the discharging current; U_4 is the voltage at the time point when the discharge is completed; U_5 is the ending voltage of the rapid-recovery process. According to the first-order resistor-capacitor circuit, the zero-input response generalization is obtained by taking U_3 and U_4 into consideration. The first-order zero-input state equation is derived from the terminal voltage for the iterative calculation process by the time constant value of . Also, different terminal voltage values are deduced at the time points k_3 and k_4, where the mathematical expressions of U_3 and U_4 are obtained, as shown in Equation (6).

$$\begin{cases} U_c = U_p e^{-\frac{k}{\tau}} \Rightarrow U = U_1 - U_c = U_1(1 - e^{-\frac{k}{\tau}}) \\ U_3 = U_1\left(1 - e^{-\frac{k_3}{\tau}}\right); U_4 = U_1\left(1 - e^{-\frac{k_4}{\tau}}\right) \end{cases} \tag{6}$$

In Equation (6), U_c is the dynamic voltage for the following period of the polarization effect; U_p is the polarization voltage; k is the discrete-time point; τ is the time constant; U is the reflected voltage; U_1 is the initial voltage at the time point of k_1. As the parameters of U_3, U_4, k_3, and k_4 are used to calculate the value of the time constant τ, the derived combination is obtained with the time constant. Then, the polarization capacitance C_p is calculated using the derivation expression shown in Equation (7).

$$\begin{cases} \tau = -\dfrac{(k_3 - k_4)}{ln\left[\dfrac{(U_1 - U_4)}{(U_1 - U_3)}\right]} \\ C_p = \dfrac{\tau}{R_p} = \dfrac{\left\{-\dfrac{(k_3 - k_4)}{ln\left[\dfrac{(U_1 - U_4)}{(U_1 - U_3)}\right]}\right\}}{R_p} \end{cases} \tag{7}$$

In Equation (7), τ is the time constant; U_1 is the initial voltage at the time point of k_1; U_3 is the voltage at the time point k_3; U_4 is the voltage at the time point k_4; R_p is the polarization resistance. The CCV increases abruptly at the time point k_1, so the voltage variation reflects the battery's internal ohmic resistance characteristics effectively. The terminal voltage U_L exhibits a gradually decreasing change tradition from the time point k_2 to k_3. According to the Kirchhoff's voltage law, the polarization capacitor C_p makes the terminal voltage decrease. As inversely determined, the polarization voltage U_p increases slightly from 0.00 V to the terminal voltage. The zero-input response of k_2 is finished until the time point k_5, in which C_p is slightly attenuated while U_p decreases gradually.

2.2. Collaborative parameter identification

By the analysis of the influencing parameters, a collaborative identification is applied to the estimation process for both the BEEC model and performance comparison. An improved estimation observer is established to form the online collaborative model parameter identification under the influence of dynamic working conditions. Based on the characteristic modeling, a state-space equation is obtained. Then, an adaptive parameter adjustment is introduced to realize the state-space equation of the battery characteristics, including environmental changes and the aging process. Also, the weight coefficients are assigned using the observed and priori state values. Time and state updates are performed through recursive calculation and feedback correction strategies. A real-time CCV measurement is carried out to achieve an accurate target state estimation and correction to improve the adaptability of collaborative estimation. The schematic diagram of the voltage state evaluation and iterative calculation procedure is constructed, as shown in Figure 3.

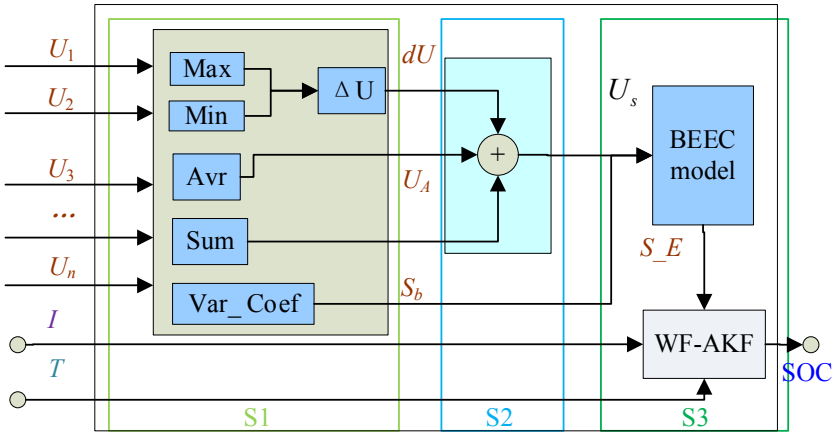

Figure 3. Schematic diagram of the voltage state evaluation and iterative calculation

In **Figure 3.**, the average voltage, variance coefficient, and rate of voltage change for the internally connected battery cells are expressed as U_A, S_b, and dU, respectively. Firstly, U_A, S_b, and dU are calculated by measuring the battery cell voltages. Then, the effective average cell voltage U_s is obtained according to the funcional calculation.

Taking U_s and S_b as input parameters, the corresponding state-space equation S_E is obtained with its variables. Then, the individual real-time measured cell voltage parameters U_1, U_2, U_3, ..., U_n, and I_L under the operating influence are used as the main input parameters for the collaborative state estimation. Combined with temperature T signal correction, the WF-AKF algorithm is established for the iterative calculation.

The specificity of dynamic group applications is analyzed using the ECM and the state-space equation. The key parameter is identified during the state estimation process. An influencing factor correction strategy is introduced for the working characteristic modeling by the theoretical analysis of the key parameters, including charge-discharge current, temperature, cycling life, self-discharge rate, and cell-to-cell consistency. Then, the WF-AKF is used for the multiple inputs and highly non-linear characteristics. The nonlinear transformation is conducted for the mean-covariance state equations, and the operating characteristics of the battery system are described under dynamic working conditions.

For the adaptive online model parameter identification, the overall structure is divided into three units, including S_1, S_2, and S_3. The input parameters are the individual battery cell voltages U_1, U_2, U_3, ..., U_n, which are transformed into a mathematical state-space equation. The WF-AKF algorithm is used for real-time iterative calculation with the results of collaborative state estimation. Input parameters are voltage, current, and temperature signals. The module average is used to obtain the average voltage U_A, as shown in Equation (8).

$$\begin{cases} U_A = (U_1 + U_2 + U_3 + \cdots + U_n)/n \\ U_{max} = Max(U_{A1}, U_{A2}, U_{A3}, \cdots, U_{An}) \\ U_{min} = Min(U_{A1}, U_{A2}, U_{A3}, \cdots, U_{An}) \\ dU = U_{max}/U_{min} \end{cases} \tag{8}$$

In Equation (8), n is the number of series-connected battery cells, where the parallel cells are used for the capacity expansion as a single battery cell. U_1, U_2, U_3, ..., U_n are CCV parameters of the connected battery

cells. U_{A1}, U_{A2}, ..., U_{An} are used for the calculation of the averaged voltage U_A. U_{max} is the maximum voltage of the internally connected battery cells, and U_{min} is their minimum voltage, according to which the differential voltage dU is calculated. Also, the SOB value is obtained, as shown in Equation (9).

$$SOB = \varepsilon = \theta^2 = \frac{1}{n}\sum_{k=1}^{n}\left(\frac{U_k - U_A}{U_A}\right)^2 \tag{9}$$

In Equation (9), the SOB condition is characterized by the variance parameter ε, which is obtained by squaring the standard deviation factor θ. U_k is the acquisition voltage of each battery cell with the assigned parameter, which is obtained at a current time point, and U_A is the average voltage. The average voltage and change rate are combined to obtain an effective average voltage U_s, which is calculated through the functional relationship and CCV difference. The estimated voltage replaces the measured value to be used for the subsequent iterative calculation, as shown in Equation (10).

$$U_s = h(dU, U_A, U_L) \tag{10}$$

In Equation (10), $h(*)$ is a function of obtaining the effective mean voltage, in which the differential voltage dU, averaged voltage U_A, and CCV value U_L are taken into consideration. In the $S3$ section, the input parameters are measured for the individual cell voltages U_1, U_2, U_3, ..., U_n with the current I_L and the SOB parameter ε. Also, the mathematical description of the state-space equation is realized by combining the correction of temperature T and the aging factor η. By making full use of the lithium-ion battery output signal characteristics, the information contained in the real-time measurement is retrieved to realize the effective expression combined with the signal change rate variation to improve the collaborative estimation adaptability. The monotonous increasing voltage is adopted with the cut-in computing direction, where the gradual approximation is realized with the dichotomy iteration flowchart, as shown in Figure 4.

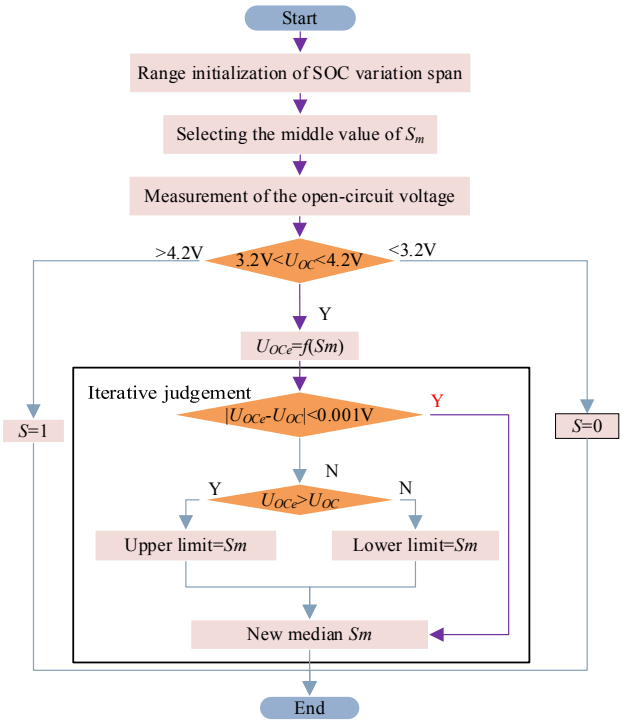

Figure 4. Flowchart of the predictive iteration voltage of the median SOC calculation

In Figure 4, the SOC variation span is initialized for the first time point, where the middle SOC value is calculated by the arithmetic average processing. By conducting the OCV measurement, the U_{oc} value is obtained, and the initial judgment is conducted for the special condition to be higher than 4.20 V or lower than 3.20 V. Then, the median search method is conducted by iterative calculation and judgment. The main implementation process is described as follows.

(1) The initial value is set as (0, 1), and the interval median parameter S_m is taken as the initial estimation factor.

(2) The measured U_{oc} value is introduced into the correction step of the whole iterative calculation process. Firstly, it should be determined whether the battery is full or empty. If true, then iterate calculation returns 1 or 0 as an output directly and exits the calculation procedure. If not, the calculation process goes to the next step.

(3) The estimated S_m value is introduced into the voltage functions to obtain the estimated value of U_{oce}.

(4) It should be judged whether the absolute difference value of ΔU between U_{oce} and U_{oc} is greater than the specified deviation range, which is set as 1 mV. When the absolute difference value of ΔU is bigger than the threshold value, the procedure continues to the next step. If not, it turns to the direct output current S_e, exiting the calculation procedure.

(5) The sizes of U_{oce} and U_{oc} are compared accordingly. If it is larger than U_{oc}, the parameter variation range is shortened, and the upper limit of the current median is reduced. Whereas, if the value of U_{oc} is large, the upward interval is shortened, and the lower limit of the medium value increases.

(6) The median factor S_m is updated to a new interval, which returns to the third step that is introduced into the OCV-SOC function again.

The cycling calculation procedure continues until the existing condition is achieved, in which ΔU is not greater than the specified deviation. A collaborative estimation framework is constructed for all model parameters based on the mechanism exploration of the EKF-UKF algorithm. The output parameters are considered for different environmental conditions, thereby realizing an accurate mathematical description of the operating characteristics. The parameter influence is adapted, including working conditions and aging factors, according to which the collaborative SOC estimation is achieved.

2.3. Multi-scale state of charge estimation

Combined with the model parameter identification, a multi-time-scale estimation model is established with an adaptive iterative calculation by considering the ambient temperature and complex current rate conditions. Then, the implementation strategy is explored to realize the real-time optimization when the lithium-ion batteries are working under different conditions with a wide temperature range. Real-time identification results are introduced,

taking the model parameters as input to optimize the wide temperature range with multiple constraints. The relationship between the performance degradation and the internal parameters is accurately obtained based on the aging degree, performance degradation, and model parameters.

The weighted data points are introduced into the iterative calculation to approximate the n-dimensional samples used to calculate the nonlinear functions. Then, an updated value is obtained by the state-space equation to achieve the goal of tracking the target battery state, so that the collaborative estimation and the internal resistance estimation are realized for real-time battery management systems. An accurate model is obtained by adaptively adjusting the measurement noise to the uncertainty noise. Therefore, the error range is controlled within a small margin to improve the stability and convergence effect. Also, the capacity decline and internal resistance increase are used as the state evaluation indexes to realize the calculation, as shown in Equation (11).

$$\Phi = \left(\frac{Q_{max}}{Q_{new}} + \frac{R_{int}}{R_{new}}\right) \Big/ 2 \tag{11}$$

In Equation (11), Φ is the aging state for the iterative calculation and evaluation; Q_{max} is the maximum discharging capacity; Q_{new} is the maximum discharge capacity of the new battery; R_{int} is the internal resistance of the current time point; R_{new} is the internal resistance of the new battery. An improved adaptive iterative calculation model is constructed, in which R_{int} is corrected in real-time with high accuracy. Therefore, the iterative calculation for the collaborative state estimation is improved. The changes of R_{int} and Q_{max} are used to characterize the aging degree, which improves the estimation accuracy effectively. As a function of the dependent variable voltage, the state value is calculated precisely as a nonlinear high-order polynomial function with explicit inverse characteristics. The systematic discrete state-space equation is built by the (ampere hour) Ah integral method, as shown in Equation (12).

$$S_k = S_{k-1} - \frac{\eta I_{k-1}}{Q_N} + w_{k-1} \tag{12}$$

In Equation (12), S_k is the SOC value at the time point k; S_{k-1} is the SOC value at the time point $k-1$; η is the Coulomb efficiency that considers both current rate and temperature; I_{k-1} is the current at the time point $k-1$; Q_N is the rated capacity of the battery; w_{k-1} is the process noise value at time point $k-1$. The independent variables are measured by the coordinate conversion and iterative binary when the dependent variable voltage is obtained. The WF-AKF estimation is established by the Ah integral method and equivalent circuit modeling. The state-space description is reflected by the observation equation by considering the time-domain Kirchhoff's voltage law of the electrical ECM, as shown in Equation (13).

$$U_{L,k} = f(S_k) - I_k R_0 - U_{pk} + \upsilon_k \tag{13}$$

In Equation (13), $U_{L,k}$ is the CCV at the time point k; $f(S_k)$ is the mathematical function for the OCV-SOC relationship so that the U_{oc} is expressed by the SOC parameter S_k at the time point k; I_k is the current at the time point k; R_0 is the internal ohmic resistance of the battery. The improved procedure is designed to extract the processing and observing noises, which are used to estimate the system's state. Afterward, the voltage across the polarization capacitor is described by U_p, which is used as the state quantity by introducing $X_k = [S_k, U_{pk}]^T$. The terminal voltage U_L is taken as an output parameter, and the current is set as an input, so the state-space equation is established accordingly, as shown in Equation (14).

$$\begin{bmatrix} U_{p(k+1)} \\ S_{k+1} \end{bmatrix} = \begin{bmatrix} exp\left(\frac{-D_k}{k}\right) & 0 \\ 0 & 1 \end{bmatrix} \times \begin{bmatrix} U_{pk} \\ S_k \end{bmatrix} + \begin{bmatrix} \frac{D_k}{C_p} \\ R_p\left[1 - exp\left(\frac{-hD_k}{Q_N}\right)\right] \end{bmatrix} I_k \tag{14}$$

In Equation (14), $U_{p(k+1)}$ is the polarization voltage at the time point $k+1$; S_{k+1} is the SOC value at the time point $k+1$; D_k is the discrete-time interval; U_{pk} is the polarization voltage at the time point k; S_k is the SOC value at the time point k; C_p is the polarization capacitance; R_p is the polarization resistance; h is the weighting coefficient; Q_N is the rated capacity of the battery; I_k is the current at the time point k. Subsequently,

an improved calculation model is constructed to correct the variance between process and measurement noises, so that the state update is realized. In the iterative calculation, the unscented transform processing is realized based on the collaborative SOC and ohmic resistance estimations. The parameters are identified in real-time in the form of a looped iteration, and the collaborative state estimation is realized. The improved calculation is realized by combining the unscented transformation and the Kalman filtering method. Afterward, an appropriate sampling strategy is used to approximate the state variable distribution. As the battery system linearization is not forced, the error calculation is avoided by ignoring the high order terms and the time-varying Jacobian matrix. Consequently, the estimation requirement is highly reduced with the adaptive correction. It is superior to carry out the state estimation methods in terms of the estimation error in which the covariance is updated using Equation (15).

$$P_{k|k} = (E - K_k C_k) P_{k-1} \tag{15}$$

In Equation (15), the error covariance $P_{k|k}$ is obtained for the time point k as a state variable; P_{k-1} is the estimated error covariance at the time point $k-1$, obtained from the error covariance at the time point $k-1$; K_k is the Kalman gain; E is an identity matrix. The state variable and covariance time-updating are investigated by the mathematical relationship, as shown in Equation (16).

$$\begin{cases} \hat{x}_{k|k} = A_{k-1}\hat{x}_{k-1|k-1} + B_{k-1}u_{k-1} \\ S_{k|k-1}^{T} \xleftarrow{QR} \begin{bmatrix} S_{k-1}^{T} A_{k-1}^{T} \\ (Q_{k-1}^{1/2})^{T} \end{bmatrix} \end{cases} \tag{16}$$

In Equation (16), $\hat{x}_{k|k}$ is the corrected state variable conducted at the time point k; $\hat{x}_{k-1|k-1}$ is the estimated at the time point $k-1$ that is calculated from the optimal state variable toward the estimation. When calculating the equation, only half of the significant values are needed to get the same estimation accuracy. According to the dependence on the initial value and the calculation stability, a square root decomposition of the state covariance matrix is introduced into the calculation process, which corrects the initial value adaptively. The

error variance matrix P_k is decomposed by $P_k = S_k S_k^T$ instead of the covariance matrix, updating the covariance decomposition matrix S_k iteratively. The corresponding calculation change of the Kalman gain is obtained, as shown in Equation (17).

$$\begin{cases} K(k) = S_{k|k-1} F_k \alpha_k, \alpha_k = [{F_k}^T F_k + R_v]^{-1} \\ F_k = {S^T}_{k|k-1} C_k, \gamma_k = \dfrac{1 \pm \sqrt{\alpha_k R_v}}{1 - \alpha_k R_v} \end{cases} \tag{17}$$

In Equation (17), $K(k)$ is the Kalman gain at the time point k; $S_{k|k-1}$ is the estimated SOC value from the time point $k-1$ to k; F_k is the forgetting factor at the time point k; α_k is the coefficient at the time point k; R_v is the error covariance; C_k is the covariance at the time point k; γ_k is the correction coefficient that is obtained by taking both α_k and R_v. As the number squaring method requires more digits in the mathematical representation, the update of the mean covariance error matrix P_k needs more valid data bits than the state quantity x to ensure the calculation accuracy. The square root calculation decomposes the mean square error matrix P_k. The state variables and covariance measurement updates are conducted by the estimation and correction strategy, as shown in Equation (18).

$$\begin{cases} \hat{x}_{k|k} = \hat{x}_{k|k-1} + K_k(y_k - C_k \hat{x}_{k|k-1} - D_k u_k) \\ S_k = S_{k|k-1}[I - \alpha_k \gamma_k F_k {F_k}^T] \end{cases} \tag{18}$$

In Equation (18), $\hat{x}_{k|k}$ is the estimated state value at the time point k; $\hat{x}_{k|k-1}$ is the estimated value given the time point $k-1$ to k; K_k is the Kalman gain at the time point k; y_k is the measured state value; C_k and D_k are the matrices of the state parameters; S_k is the estimated SOC value at the time point k; $S_{k|k-1}$ is the estimated SOC value from the time point $k-1$ to k. The parameters of α_k, γ_k, and F_k are calculated according to Equation (17). The error covariance matrix P_k is decomposed to be guaranteed as a non-negative definite, overcoming the filtering divergence problem caused by the uncertainties of the estimation system. As linked to a particle filter, the algorithm has a significant advantage compared with Monte Carlo and approximate Bayesian algorithms in predicting the dynamic battery parameters accurately.

2.4. Influencing factor optimization and correction

The performance evaluation procedure for collaborative state estimation is established to complete the preliminary realization of related algorithms. Consequently, the estimation effect improves with the convergence performance. The collaborative performance evaluation is investigated for state estimation, correctness, verification, stability, and consistency testing. The online collaborative state estimation is realized for the state quantities based on the preliminary performance evaluation. The functional relationship is described mathematically for the ECM, including SOC, SOB, and aging characteristics.

The weighting factor correction is implemented by calculating the voltage variation coefficient. The mathematical SOB expression is obtained and applied in the correction steps. Also, the SOB evaluation is introduced into the correction process, in which the external battery characteristics are mainly affected by the current, capacity difference, and initial state variation. The CCV value is used as a comprehensive reflection of the model parameter and state factor changes. The values of external factors such as U_L, I, and T are measured, and the evaluation is implemented accordingly. The numerical description is conducted, and the correction strategy is combined to improve the estimation accuracy. A mathematical expression is applied to the correction steps by calculating the voltage variation coefficient.

Combined with the correction strategy of the environmental condition influence, the differences between internally connected battery cells are described, and the construction problem is solved. Through the influence degree of each input factor, the weighting preset of each parameter is realized in the evaluation process to carry out the real-time correction and iterative calculation. A numerical SOB evaluation is conducted for the state parameter correction with the model parameters and weighting factor correction. A numerical description is conducted to improve the estimation accuracy and is introduced into the equivalent circuit modeling process to

realize the correction effectively.

The ECM and collaborative state estimation are realized in the correction steps. Based on the selected wide temperature range conditions, the SOC estimations are conducted and analyzed. A balanced charging strategy is used to maintain the initial value at full capacity, and the change characteristic is normalized by Q_N. As the aging process changes slowly, the functional relationship is determined through periodic measurement and calibration. The functional relationship of ΔQ_N with time is obtained through the number correction of superimposed cycles simultaneously. The correction of Q_{rated} is conducted by considering the cycling number. Also, the corrected capacity Q_N is obtained for Q_{rated} with the aging factor by the superimposing effects.

3. Experimental analysis

A multi-level model is constructed to realize the collaborative state estimation of lithium-ion batteries that are suitable for complex working environments with stability analysis. The performance evaluation of the proposed iterative calculation algorithm is investigated effectively. Due to the development of battery management systems, embedded verification is realized for the ECM and collaborative SOC estimation. The experimental analysis of working condition influence is carried out by considering the measurement accuracy of different initial state quantities and input parameters. Multiple current rates combined with working condition experimental results are performed to obtain a dynamic relationship between the temperature change and the output parameters in the model.

3.1. Experimental platform for the time-varying temperature and current rate test

The battery testing platform is constructed to evaluate the performance of the designed model throughout the experimental analysis, which verifies the accuracy of the theoretical analysis. The experimental battery samples

are established under different SOB scenarios and the operating mode simulation to analyze characteristic changes under time-varying conditions. The experimental testing platform under complex working conditions is constructed, as shown in Figure 5.

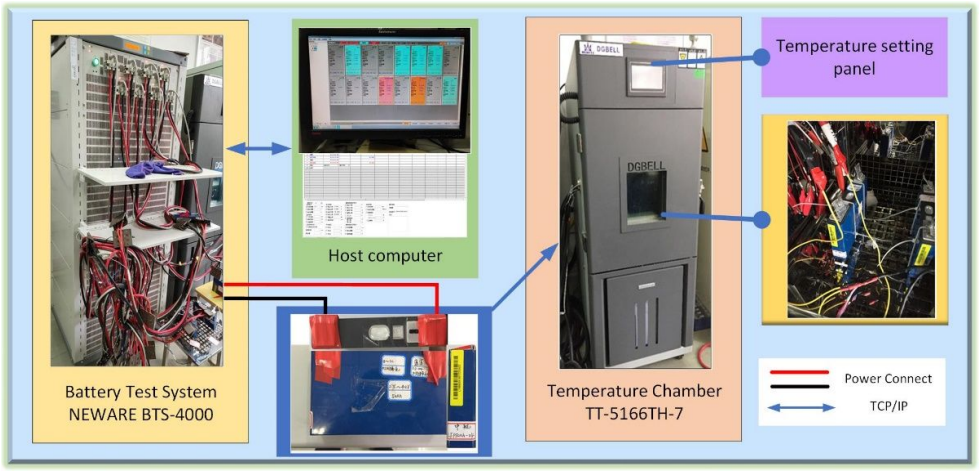

Figure 5. Experimental testing platform under time-varying ambient temperature and current rates

In Figure 5, the experimental testing platform is constructed using a lithium-ion battery (AVIC CFP50AH), a charge-discharge tester (BTS200-100-10-4), and a temperature chamber (DGBELL BTT-331C), which are connected by the TCP/IP Fieldbus control system. The testing current rate and working conditions are controlled by an industrial personal computer (IPC) that is connected to the equipment by a peripheral network cable. The parameter identification and state estimation effect verification are performed under different working conditions. Since the battery adopts the constant voltage charging method after the constant current application, the charging time is relatively easy to estimate. Therefore, the parameter identification is combined with a composite pulse-power test.

3.2. Core parameter changing factor under temperature variation

The battery characteristics are obtained for different temperature conditions. When the SOC value varies from 1 to 0.2, the internal resistance is relatively stable with an insignificant change. When the SOC value varies from

0.2 to 0.1, the internal resistance increases rapidly. When the SOC value is lower than 0.1, the internal resistance increases rapidly and doubles. The internal resistance variation characteristics are the same when the temperature varies from -20 to 40 °C, which increases gradually, with temperature changes and rapidly when the temperature decreases. The relationship between the parameter and capacity-temperature variation is obtained, as shown in Figure 6.

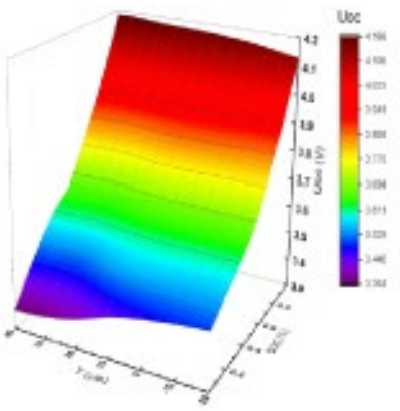

(a) Variation of the open-circuit voltage

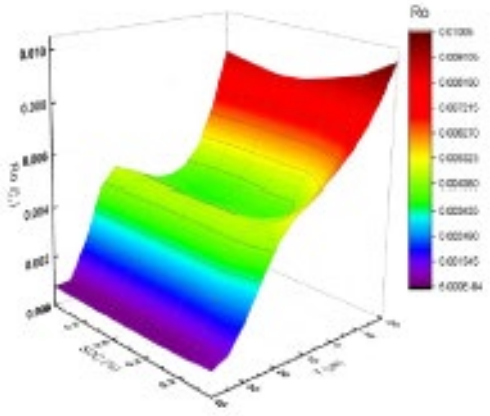

(b) Variation of the internal resistance

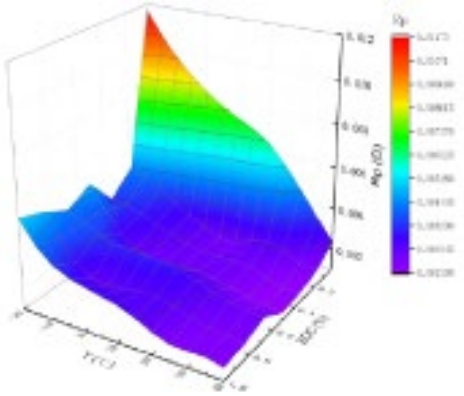

(c) Variation of the polarization resistance

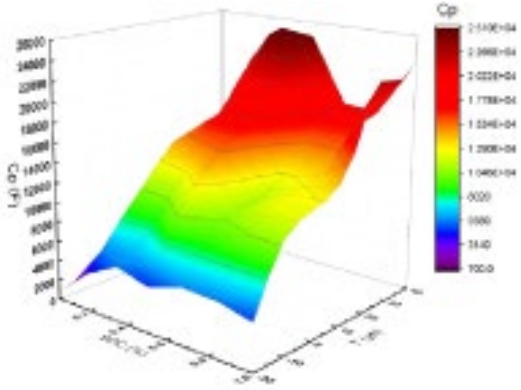

(d) Variation of the polarization capacitance

Figure 6. Relationship of parameters under capacity and temperature variations

In Figure 6., under low-temperature conditions, the CCV value of the battery reaches the cut-off voltage quickly. The ohmic resistance under negative temperature conditions shows an increasing trend, but it decreases uniformly from the positive to the highest temperature. The trackability of the

proposed algorithm tracks the changes of real values well under complex BBDST working condition. During the whole operation period of the lithium-ion battery, the maximum estimation error is 0.87%. Meanwhile, the estimated SOC value obtained by the Ah integral method still has a high deviation. The estimation effect if investigated when the initial state value is inaccurate to analyze the iterative calculation adaptability. This method has a strong self-correction capability, and the output waveform converges to avoid the estimation error of the actual value curve within a limited sampling period. As a result, a verification of the experimental results is obtained under the complex condition, as shown in Figure 7.

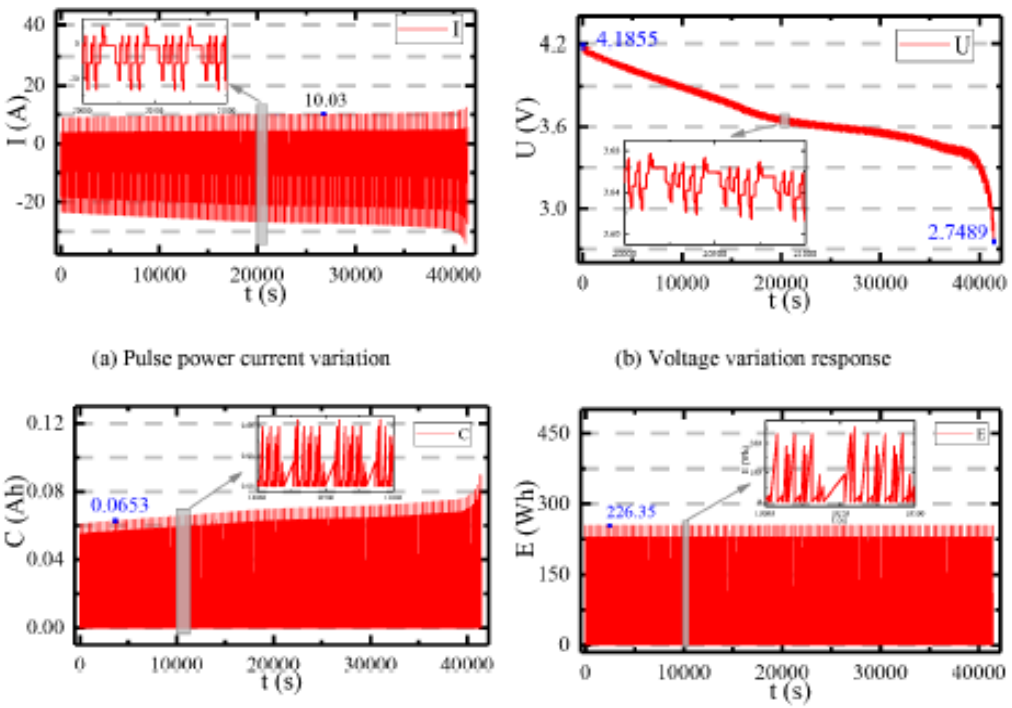

(a) Pulse power current variation

(b) Voltage variation response

(c) Capacity variation response

(d) Energy variation response

Figure 7. Experimental results under the complex BBDST working condition

In Figure 7. Subfigure (a) is the pulse power current variation under the complex BBDST working conditions; subfigure (b) is the responding voltage variation that varies from the full to the empty capacity state: subfigure (c)

is the capacity variation response; subfigure (d) is the energy variation response. Based on the ECM of the lithium-ion battery, the iterative calculation model is built, and a decoupling iterative Kalman filtering algorithm is written in the *S*-function to realize the accurate state estimation. The estimation results are verified by the experimental test under complex working condition.

3.3. Pulse current condition voltage tracking results

A high polarization resistance under decreasing temperature conditions with low values of 0.10 is observed. The parameter values obtained for the charge and discharge processes are averaged as the model parameter value suitable for different SOC levels. The highest polarization parameter values are recorded in the negative temperature range. The polarization resistance and capacitance are dependent on the terminal voltage. There is an increase in polarization capacitance with increasing temperature, in which the highest value is obtained under high-temperature conditions. Based on the parameter identification result, the experimental terminal voltage comparison and error curves for the main charge and main discharge conditions are obtained, as shown in Figure 8.

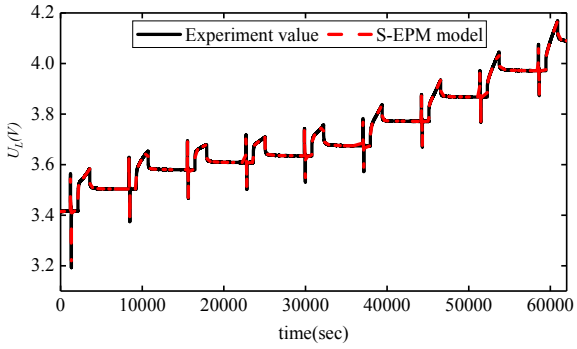

(a) Main charge terminal voltage traction

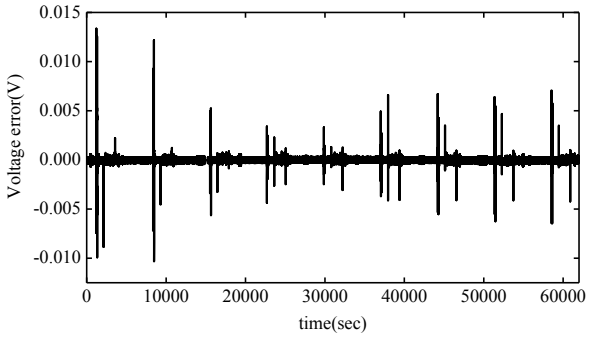

(b) Main charge voltage error curve

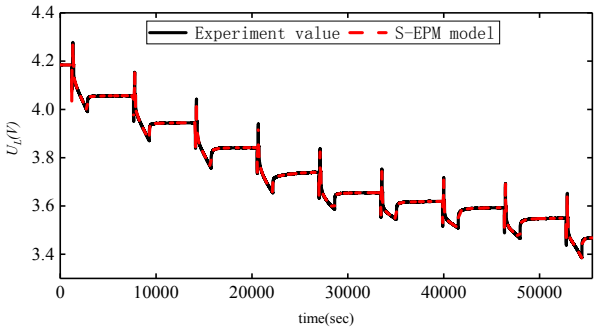

(c) Main discharge terminal voltage

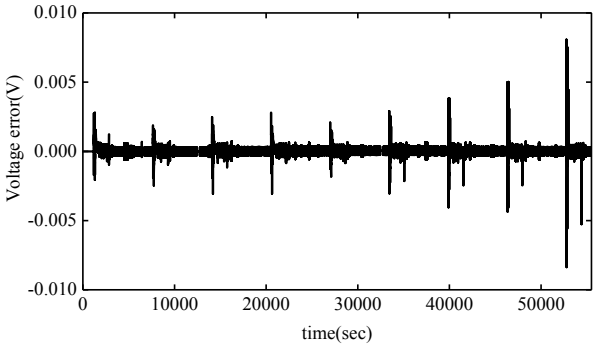

(d) Main discharge voltage error curve

Figure 8. Terminal voltage estimation for the pulse current charge and discharge tests

In Figure 8, subfigure (a) is the main charge terminal voltage traction; subfigure (b) is the main charge voltage error curve; subfigure (c) is the main discharge terminal voltage; subfigure (d) is the main discharge voltage error curve. The terminal voltage traction estimates are accurate for the whole pulse charge- and discharge processes ~~at~~ under different working conditions. In the main charging process, the maximum estimation error is less than 0.015 V with a nominal voltage of 4.20 V, so the maximum CCV traction error is 0.36%. The maximum identification error is 0.012 V in the main discharging process, with a maximum error of 0.24%. The estimated parameters are verified by tuning the relevant model parameters effectively.

3.4. Whole-life-cycle state of charge estimation

Based on the charging current provided by the lithium-ion battery's manufacturer, the battery is charged to its cut-off voltage and converted into the constant voltage charging process. The electricity mainly comes from the CC charging stage, while the CV charging stage is used to supplement the battery, so the CC mode is used for the charging conditions. Consequently, the working voltage measurement scheme is designed. (1) The discharge is conducted with a 1 C current rate before the CCV value equals 3.00 V. (2) The battery is shelved for 30 minutes. (3) The charging is conducted with a current rate of 0.2 C and stepwise to 0.05 of the rated capacity. (4) The voltage is measured after being shelved for 30 minutes. (5) The voltage is measured when the SOC value equals

0.05, 0.1, 0.15, …, 0.95 sequentially. (6) Steps (1) to (5) are repeated to obtain the CCV value for the current rates 0.3 C, 1.4 C, and 0.5C. The voltage changing curve is obtained for different current rates with the CCV difference between the internally connected battery cells for the same SOC level adaptive to the time-varying charge-discharge current rates, as shown in Figure 9.

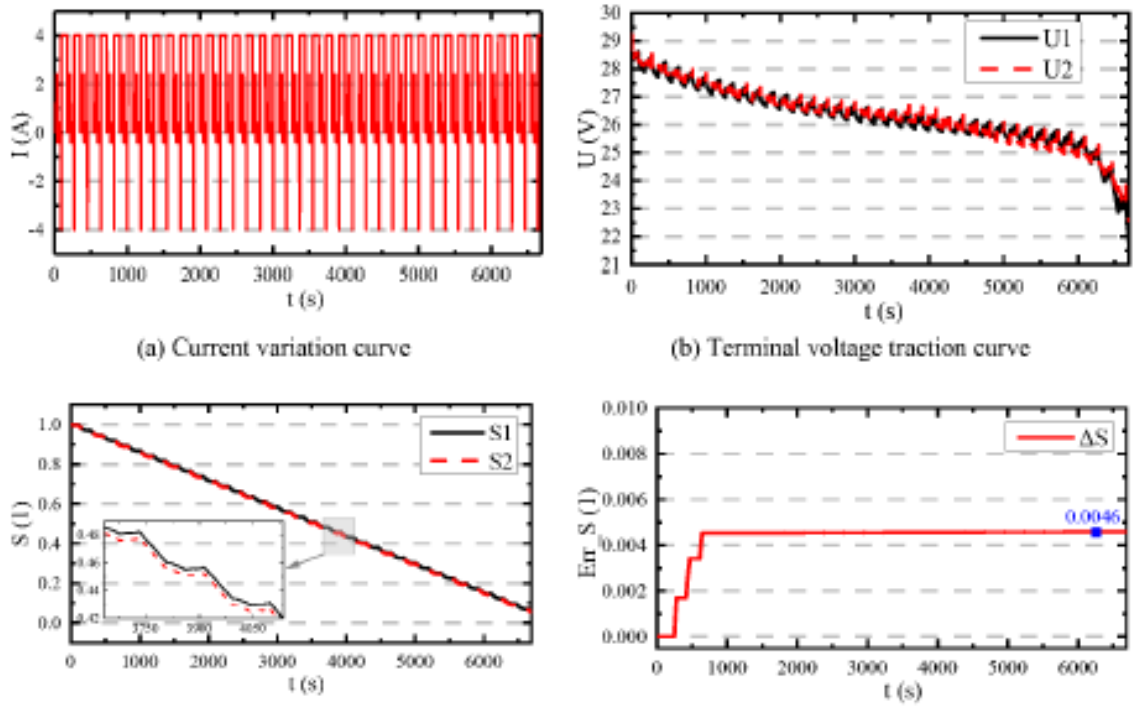

(a) Current variation curve (b) Terminal voltage traction curve

(c) SOC estimation effect comparison (d) Comparative SOC estimation error results

Figure 9. CCV traction and SOC estimation for time-varying current rates under the BBDST working condition

In Figure 9. Subfigure (a) is the SOC estimation effect comparison; subfigure (b) is the main charge voltage error distribution; subfigure (c) is the main discharge terminal voltage; subfigure (d) is the comparative SOC estimation error results. In subfigure (c), A1 is the actual SOC, and S2 is the SOC estimated by the proposed WF-AKF algorithm. It can be observed in subfigure (d) that is stabilizes the large initial SOC estimation error by tracking the actual with a maximum error of 0.46% under the complex BBDST working condition. The battery cell has a large charging current rate and an operating voltage under the same SOC conditions. When the discharge

current rate increases, the overall CCV value of the high current rate is greater than the value of the low current rate. Besides, the working characteristics have a large CCV change during the initial time points at both ends of the battery, and the variation in the discharging platform tends to be gradual. The difference in the operating voltage increases gradually to the same energy conditions as between 0.2 C, 0.3 C, 0.4 C, and 0.5 C. Based on the trend, the operating voltage change caused by the current rate of 0.1 C is smaller than 12 mV, which shows that the charging current rate changes have a great impact on the SOC estimation.

4. Conclusion

The whole-life-cycle SOC estimation is essential for lithium-ion batteries, which are difficult to realize under wide temperature range conditions. Consequently, an improved weighting factor-adaptive Kalman filtering (WF-AKF) method is proposed, combined with a bipartite electrical equivalent circuit (BEEC) model by the collaborative parameter identification strategy with time-varying factor correction for accurate SOC estimation. An adaptive multi-time-scale iterative estimation-correction model is constructed by combining equivalent circuit modeling and collaborative state estimation. The whole-life-cycle iterative calculation models and the sub-models are established for real-time state estimation by considering the temperature and current rate variations with aging characteristics. This voltage traction method is accurate, with a maximum traction error of 0.36%, showing a decreasing trend for the main pulse current charging process. The maximum CCV traction error is 0.24% for the main pulse current discharging process. It is observed that the proposed WF-AKF algorithm stabilizes the large initial SOC estimation error by tracking the actual with a maximum error of 0.46% under the complex BBDST working condition. The proposed collaborative SOC estimation method has high accuracy and robustness advantages, providing a theoretical basis for the durable and efficient operation of lithium-ion batteries.

Acknowledgments

The work is supported by the National Natural Science Foundation of China (No. 62173281, 61801407), the Sichuan Science and Technology Program (No. 2019YFG0427), the China Scholarship Council (No. 201908515099), and Fund of Robot Technology used for the Special Environment Key Laboratory of Sichuan Province (No. 18kftk03).

References

1. Ouyang, T.C., et al., *A novel state of charge estimation method for lithium-ion batteries based on bias compensation.* Energy, 2021. **226**(13): p. 1-13.

2. Shrivastava, P., et al., *Combined State of Charge and State of Energy Estimation of Lithium-Ion Battery Using Dual Forgetting Factor-Based Adaptive Extended Kalman Filter for Electric Vehicle Applications.* Ieee Transactions on Vehicular Technology, 2021. **70**(2): p. 1200-1215.

3. Chen, C.H., et al., *Development of Experimental Techniques for Parameterization of Multi-scale Lithium-ion Battery Models.* Journal of the Electrochemical Society, 2020. **167**(8): p. 1-23.

4. Shen, J.W., et al., *State of charge estimation framework for lithium-ion batteries based on square root cubature Kalman filter under wide operation temperature range.* International Journal of Energy Research, 2021. **45**(4): p. 5586-5601.

5. Shi, Y., et al., *The optimization of state of charge and state of health estimation for lithium-ions battery using combined deep learning and Kalman filter methods.* International Journal of Energy Research, 2021. **45**(7): p. 11206-11230.

6. Hennessy, M.G. and I.R. Moyles, *Asymptotic reduction and homogenization of a thermo-electrochemical model for a lithium-ion battery.* Applied Mathematical Modelling, 2020. **80**: p. 724-754.

7. Li, X., et al., *State-of-charge estimation tolerant of battery aging based on a physics-based model and an adaptive cubature Kalman filter.* Energy, 2021. **220**(119767): p. 1-13.

8. Seruga, D., et al., *Continuous modelling of cyclic ageing for lithium-ion batteries.* Energy, 2021. **215**(119079): p. 1-14.

9. Shu, X., et al., *An adaptive fusion estimation algorithm for state of charge of lithium-ion batteries considering wide operating temperature and degradation.* Journal of Power Sources, 2020. **462**: p. 1-14.

10. Wang, S.L., et al., *A novel energy management strategy for the ternary lithium batteries based on the dynamic equivalent circuit modeling and differential Kalman filtering under time-varying conditions.* Journal of Power Sources, 2020. **450**: p. 1-36.

11. Zheng, Y.J., et al., *A simplification of the time-domain equivalent circuit model for lithium-ion batteries based on*

low-frequency electrochemical impedance spectra. Journal of Power Sources, 2021. **489**: p. 1-12.

12. Zhu, J.G., et al., *Investigation of capacity fade for 18650-type lithium-ion batteries cycled in different state of charge (SoC) ranges.* Journal of Power Sources, 2021. **489**: p. 1-12.

13. Xu, W.H., et al., *A novel adaptive dual extended Kalman filtering algorithm for the Li-ion battery state of charge and state of health co-estimation.* International Journal of Energy Research, 2021. **45**(12): p. 14592-14602.

14. Nian, P., S.Z. Zhang, and X.W. Zhang, *Co-estimation for capacity and state of charge for lithium-ion batteries using improved adaptive extended Kalman filter.* Journal of Energy Storage, 2021. **40**(8): p. 1-15.

15. Qiu, X.H., W.X. Wu, and S.F. Wang, *Remaining useful life prediction of lithium-ion battery based on improved cuckoo search particle filter and a novel state of charge estimation method.* Journal of Power Sources, 2020. **450**(227700): p. 1-13.

16. Feng, F., et al., *Co-estimation of lithium-ion battery state of charge and state of temperature based on a hybrid electrochemical-thermal-neural-network model.* Journal of Power Sources, 2020. **455**: p. 1-14.

17. Wu, M.Y., et al., *State of Charge Estimation of Power Lithium-ion Battery Based on a Variable Forgetting Factor Adaptive Kalman Filter.* Journal of Energy Storage, 2021. **41**: p. 1-8.

18. Limoge, D.W. and A.M. Annaswamy, *An Adaptive Observer Design for Real-Time Parameter Estimation in Lithium-Ion Batteries.* IEEE Transactions on Control Systems Technology, 2020. **28**(2): p. 505-520.

19. Mawonou, K.S.R., et al., *Improved state of charge estimation for Li-ion batteries using fractional order extended Kalman filter.* Journal of Power Sources, 2019. **435**(2): p. 1-14.

20. Sun, D.M., et al., *State of charge estimation for lithium-ion battery based on an Intelligent Adaptive Extended Kalman Filter with improved noise estimator.* Energy, 2021. **214**: p. 1-14.

21. Lai, X., et al., *A comparative study of global optimization methods for parameter identification of different equivalent circuit models for Li-ion batteries.* Electrochimica Acta, 2019. **295**: p. 1057-1066.

22. Wei, Z.B., et al., *Noise-Immune Model Identification and State-of-Charge Estimation for Lithium-Ion Battery Using Bilinear Parameterization.* Ieee Transactions on Industrial Electronics, 2021. **68**(1): p. 312-323.

23. Thenaisie, G., C.H. Park, and S.G. Lee, *A Real-Time Entropy Estimation Algorithm for Lithium Batteries Based on a Combination of Kalman Filter and Nonlinear Observer.* IEEE Transactions on Industrial Electronics, 2020. **67**(9): p. 8034-8043.

24. Sun, B.X., et al., *Study of Parameters Identification Method of Li-Ion Battery Model for EV Power Profile Based on Transient Characteristics Data.* IEEE Transactions on Intelligent Transportation Systems, 2021. **22**(1): p. 661-672.

25. Liu, S.Q., et al., *A Novel Discharge Mode Identification Method for Series-Connected Battery Pack Online State-of-Charge Estimation Over A Wide Life Scale.* IEEE Transactions on Power Electronics, 2021. **36**(1): p. 326-341.

26. Meng, J., M. Boukhnifer, and D. Diallo, *Comparative study of lithium-ion battery open-circuit-voltage online estimation methods.* IET Electrical Systems in Transportation, 2020. **10**(2): p. 162-169.

27. Li, W.H., et al., *Online capacity estimation of lithium-ion batteries with deep long short-term memory networks.* Journal of Power Sources, 2021. **482**(228863): p. 1-11.

28. Zhou, S.D., et al., *Adaptive model parameter identification for lithium-ion batteries based on improved coupling hybrid adaptive particle swarm optimization-simulated annealing method.* Journal of Power Sources, 2021. **482**: p. 1-12.

29. Li, L., et al., *A combination state of charge estimation method for ternary polymer lithium battery considering temperature influence.* Journal Of Power Sources, 2021. **484**: p. 1-17.

30. Zhu, J.G., et al., *Investigation of capacity fade for 18650-type lithium-ion batteries cycled in different state of charge (SoC) ranges.* Journal of Power Sources, 2021. **489**(7): p. 1-12.

31. Xing, J. and P. Wu, *State of Charge Estimation of Lithium-Ion Battery Based on Improved Adaptive Unscented Kalman Filter.* Sustainability, 2021. **13**(9): p. 1-16.

32. Zhang, T., et al., *A Systematic Framework for State of Charge, State of Health and State of Power Co-Estimation of Lithium-Ion Battery in Electric Vehicles.* Sustainability, 2021. **13**(9): p. 1-19.

33. Zheng, Y.J., et al., *A novel capacity estimation method for lithium-ion batteries using fusion estimation of charging curve sections and discrete Arrhenius aging model.* Applied Energy, 2019. **251**: p. 1-13.

34. Shi, W.H., et al., *A novel voltage matching-adaptive extended Kalman filtering method for the state of charge prediction of lithium-ion batteries.* Transactions of the Institute of Measurement and Control, 2021. **7**(4): p. 1-12.

35. Wang, Q.S., et al., *A Novel Consistency Evaluation Method for Series-Connected Battery Systems Based on Real-World Operation Data.* Ieee Transactions on Transportation Electrification, 2021. **7**(2): p. 437-451.

36. Wang, D.F., et al., *Lithium-ion battery equivalent model over full-range state of charge based on electrochemical process simplification.* Electrochimica Acta, 2021. **389**: p. 1-12.

37. Xie, Y.X., et al., *Improved gray wolf particle filtering and high-fidelity second-order autoregressive equivalent modeling for intelligent state of charge prediction of lithium-ion batteries.* International Journal of Energy Research, 2021. **45**(13): p. 19203-19214.

38. Zhang, S.Z. and X.W. Zhang, *A multi time-scale framework for state-of-charge and capacity estimation of lithium-ion battery under optimal operating temperature range.* Journal of Energy Storage, 2021. **35**(6861): p. 1-16.

39. Tan, X.J., et al., *Online state-of-health estimation of lithium-ion battery based on dynamic parameter identification at multi timescale and support vector regression.* Journal of Power Sources, 2021. **484**(1): p. 1-10.

40. Wang, J.X., et al., *Improved Modeling of Lithium-Ion Battery Capacity Degradation Using an Individual-State Training Method and Recurrent Softplus Neural Network.* IEEE Access, 2021. **9**: p. 7845-7855.

41. Guo, D.X., et al., *Physics-based fractional-order model with simplified solid phase diffusion of lithium-ion battery.* Journal of Energy Storage, 2020. **30**: p. 1-11.

42. Li, Y., et al., *Lithium-ion battery capacity estimation — A pruned convolutional neural network approach assisted with transfer learning.* Applied Energy, 2021. **285**(116410): p. 1-12.

43. Chen, M.B., et al., *Performance and safety protection of internal short circuit in lithium-ion battery based on a multilayer electro-thermal coupling model.* Applied Thermal Engineering, 2019. **146**: p. 775-784.

44. Chen, G.J., et al., *Searching for the optimal current pattern based on grey wolf optimizer and equivalent circuit model of Li-ion batteries.* Journal of Energy Storage, 2021. **33**(3): p. 1-10.

45. Bruch, M., et al., *Novel method for the parameterization of a reliable equivalent circuit model for the precise simulation of a battery cell's electric behavior.* Journal of Power Sources, 2021. **490**(1): p. 1-16.

46. Hu, X.S., et al., *An enhanced multi-state estimation hierarchy for advanced lithium-ion battery management.* Applied Energy, 2020. **257**: p. 1-13.

47. Shen, S., et al., *Deep convolutional neural networks with ensemble learning and transfer learning for capacity estimation of lithium-ion batteries.* Applied Energy, 2020. **260**(114296): p. 1-14.

48. Song, Y.C., et al., *A hybrid statistical data-driven method for on-line joint state estimation of lithium-ion batteries.* Applied Energy, 2020. **261**: p. 1-13.

49. Jiang, C., et al., *A state-of-charge estimation method of the power lithium-ion battery in complex conditions based on adaptive square root extended Kalman filter.* Energy, 2021. **219**: p. 1-11.

50. Shu, X., et al., *Stage of Charge Estimation of Lithium-Ion Battery Packs Based on Improved Cubature Kalman Filter With Long Short-Term Memory Model.* IEEE Transactions on Transportation Electrification, 2021. **7**(3): p. 1271-1284.

51. Geng, Z.Y., et al., *Bridging physics-based and equivalent circuit models for lithium-ion batteries.* Electrochimica Acta, 2021. **372**(9): p. 1-9.

52. Lai, X., et al., *Capacity estimation of lithium-ion cells by combining model-based and data-driven methods based on a sequential extended Kalman filter.* Energy, 2021. **216**: p. 1-14.

53. Xiao, B., B. Xiao, and L.S. Liu, *Rapid measurement method for lithium-ion battery state of health estimation based on least squares support vector regression.* International Journal of Energy Research, 2021. **45**(4): p. 5695-5709.

54. Zheng, Y.J., et al., *State-of-charge inconsistency estimation of lithium-ion battery pack using mean-difference model and extended Kalman filter.* Journal of Power Sources, 2018. **383**: p. 50-58.

55. Tang, X., et al., *Aging trajectory prediction for lithium-ion batteries via model migration and Bayesian Monte Carlo method.* Applied Energy, 2019. **254**(113591): p. 1-12.

56. Shi, H.T., et al., *Improved splice-electrochemical circuit polarization modeling and optimized dynamic functional multi-innovation least square parameter identification for lithium-ion batteries.* International Journal of Energy Research, 2021. **45**(10): p. 1-15.